

STORAGE OF CRYSTALLINE ION BEAMS *

U. Schramm [†], T. Schätz [‡], M. Bussmann, D. Habs
 Sektion Physik, LMU Munich, D-85748 Garching, Germany

Abstract

Recently, the phase transition of a low-energy $^{24}\text{Mg}^+$ ion beam into the Coulomb-ordered ‘crystalline’ state could be realized in the rf quadrupole storage ring PALLAS at the LMU Munich. Thereby, an increase of the phase space density of the beam, subjected to longitudinal laser cooling, by about six orders of magnitude was observed. In this paper, we focus on the systematic experimental investigation of the role of the focusing conditions and of bending shear in the storage ring on the attainment of crystalline beams of different crystal structure.

CRYSTALLINE BEAMS

Almost two decades after the first discussion of the ‘crystallization’ [1, 2, 3, 4] of stored ion beams into a Coulomb-ordered state, this phase transition could recently be realized in the table-top rf quadrupole storage ring PALLAS (PAul Laser CoolIng Acceleration System) for coasting [5, 6, 7] and for bunched ion beams [8, 9]. The phase transition of a space-charge dominated ion beam to the ‘crystalline’ state can occur when the mutual Coulomb-energy of the ions overcomes their mean kinetic energy by about two orders of magnitude [1, 7]. As typical inter-ion distances of stored singly charged ions amount to of the order of $10\ \mu\text{m}$, beam temperatures in the range of mK are required. This temperature range can be reached with laser cooling [10] provided that heating mechanisms as intra-beam scattering (IBS) [11, 12] in the emittance-dominated ‘gaseous’ regime are sufficiently reduced. This can be achieved either by a strong dilution of the ion beam, as demonstrated by experiments on electron-cooled heavy ion beams [13, 14, 15] and on laser-cooled $^9\text{Be}^+$ beams [16], or by minimizing modulations of the beam envelope, which has been realized with PALLAS.

The crystalline state of an ion beam represents the state of ultimate brilliance in the sense that for given focusing strength and ion current, ultimate phase space densities are reached [5]. Moreover, crystalline beams were found to be rather insensitive to the strong heating mechanisms (IBS) omnipresent in the non-crystalline regime [5, 6]. As these mechanisms rely on dissipative Coulomb collisions, they are strongly suppressed in the crystalline regime [2, 11, 12, 17]. Even without further cooling, no significant emittance growth was experienced for crystalline beams for typically 10^6 focusing periods [5, 18].

Yet, the inevitable modulation of the beam envelope in the alternating fields of a storage ring and velocity de-

pendent shear forces have been predicted to complicate the maintenance of crystalline structures larger than a one-dimensional (1D) string of ions [2, 17, 19]. In this paper, the focusing conditions for which crystalline beams are attainable in PALLAS are therefore discussed as a function of the ion beam velocity. Another issue is that longitudinal laser cooling itself, due to the randomness of photon scattering, may cause transverse instabilities of crystalline beams [18], as this effect has been proposed [20] to have hindered the crystallization of dilute ion beams in the storage rings ASTRID (Aarhus) and TSR (Heidelberg) [16].

EXPERIMENTAL TECHNIQUES

A sketch of the low-energy table-top rf quadrupole storage ring PALLAS [21] is given in Fig. 1.

Experimental Setup

For the transverse confinement and simultaneous bending of a low-energy $^{24}\text{Mg}^+$ ion beam, an rf voltage U_{rf} of several 100 V is applied between the quadrupole ring electrodes, depicted in Fig. 1, at a frequency $\Omega = 2\pi \times 6.3\ \text{MHz}$. The alternating quadrupole field leads to a bound periodic motion of the stored particles at the secular frequency $\omega_{sec} = q\Omega/\sqrt{8}$ superimposed by a fast quiver motion (micro-motion) at the driving frequency Ω , where $q = 2eU_{rf}/(m\Omega^2r_0^2)$ denotes the stability parameter of the underlying Mathieu differential equation, e and m stand for the charge and mass of the $^{24}\text{Mg}^+$ ions, $r_0 = 2.5\ \text{mm}$ for the aperture radius of the quadrupole channel.

Similar to the more common case of an ion storage ring consisting of a periodic lattice of bending and focusing magnets, the transverse confinement of the ion beam in the rf quadrupole storage ring PALLAS can be characterized by the period length of the confining force and the corresponding transverse ion motion. The number of focusing sections per revolution, the periodicity P , corresponds to the number of rf cycles per revolution $P = \Omega/\omega_{rev} = \Omega R/v$ and the number of transverse betatron oscillations, the storage ring tune Q , to the number of secular oscillations in the rf field $Q = \omega_{sec}/\omega_{rev} = \omega_{sec}R/v$. Notably, both quantities become velocity dependent in contrast to the case of magnetic confinement. For a typical beam velocity of $v = 2800\ \text{m/s}$, the periodicity amounts to $P \approx 800$. Although the absolute focusing strength of the rf electric focusing is comparatively strong in PALLAS ($\omega_{sec} = 2\pi \times 390\ \text{kHz}$ for $Q = 50$), the phase advance per lattice cell $2\pi \times Q/P$ and thus the envelope modulation of the beam remains moderate.

After the loading of the ring with a cloud of ions [6], the resonant light pressure of the continuously tuned co-

* supported by DFG (HA-1101/8) and MLL

[†] email: ulrich.schramm@physik.uni-muenchen.de

[‡] present address: NIST Boulder, USA

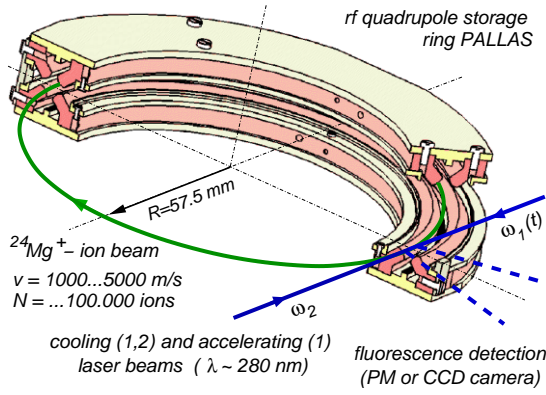


Figure 1: Schematic view of the table-top rf quadrupole storage ring PALLAS. The design orbit of the ion beam is defined by concentric ring electrodes in quadrupole geometry (aperture radius $r_0 = 2.5$ mm). Two counter-propagating laser beams are overlapped tangentially with the ion orbit.

propagating laser beam (frequency $\omega_1(t)$) is used to accelerate a non-crystalline $^{24}\text{Mg}^+$ ion ensemble to a beam velocity v defined by the fixed frequency ω_2 of the counter-propagating laser beam, as sketched at the bottom of Fig. 2 and described in [5, 6]. The *longitudinal* velocity spread of the ion beam is efficiently reduced by the friction force, resulting from the combination of both accelerating and decelerating forces. No direct damping of the *transverse* ion motion is applied which therefore has to rely on the coupling of the transverse to the longitudinal motion by the inter-particle Coulomb interaction.

Ion Beam Crystallization

The fluorescence signal emitted by a non-crystalline beam ($q = 0.2$) as a function of the relative detuning $\Delta\omega_1(t)$ of the co-propagating laser beam (and thus of the beam velocity v) is shown in Fig. 2. The behaviour drastically changes when the focusing strength is raised and the coupling between the ions is enhanced (grey curve at $q = 0.31$). The signal first increases corresponding to the cooling of the initially non-crystalline beam. Then, at $\Delta\omega_1(t) \approx -25\Gamma/2$, the signal decreases and subsequently rises to a sharp peak. At last, the rate drops off when the forces of the two laser beams compensate ($\Delta\omega_1(t) \equiv 0$). For the ion current discussed here, this signature of the ‘dip’ in the fluorescence signal is characteristic for the phase transition to a crystalline beam. It can be understood as a vanishing of the rf heating (IBS) in the gaseous regime which also caused the broadening of the velocity spread. With slightly reduced rf heating the phase transition sets in earlier. The characteristic ‘dip’ cannot be resolved any more (black curve at $q = 0.31$).

The phase transition to the crystalline beam is further pinpointed by the sudden decrease of the transverse beam size to the size of a linear string of ions [5, 6], demonstrated with the images inserted in Fig. 2.

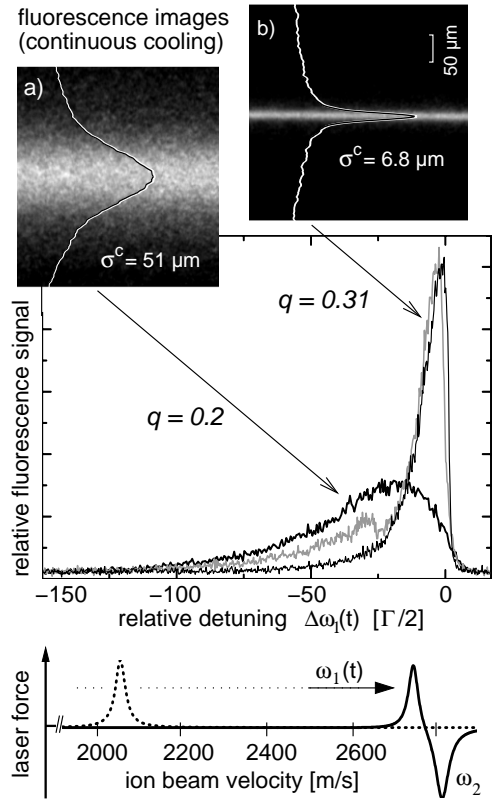


Figure 2: Fluorescence signal of an ion beam ($N = 18,000$) as a function of the relative detuning $\Delta\omega_1(t)$ of the co-propagating laser beam in terms of half the natural transition line width $\Gamma = 2\pi \times 42.7$ MHz. In this non-stationary cooling regime, used also for the acceleration of the ions as sketched below, the laser frequency $\omega_1(t)$ is tuned at a typical rate of about $50\Gamma/\text{s}$. With an increase of the focusing strength ($q = 0.2 \rightarrow 0.31$) the phase transition is induced. The signal changes markedly as described in the text and further displayed in the inserted fluorescence images, recorded at constant detuning.

Properties of Ion Crystals

The structure of crystalline ion beams was first studied in MD simulations [22] and observed in experiments with elongated *stationary* ion crystals in ring-shaped [23, 5, 7] and linear [24] rf quadrupole traps. It was found to uniquely depend on the dimensionless linear density $\lambda = N/(2\pi R) \times a_{ws}$ expressed in terms of the Wigner-Seitz radius $a_{ws} = [1/(4\pi\epsilon_0) \times 3e^2/(2m\omega_{sec}^2)]^{1/3}$ to account for the dominant influence of the charge neutralizing confining potential on the average ion density. The structure develops with rising λ from a string of ions for $\lambda < 0.71$ over a zig-zag band into three-dimensional helical structures, as later illustrated with Fig. 4. Also dynamic properties of the ion crystal as the plasma frequency $\omega_p = \sqrt{2}\omega_{sec}$ are determined by the focusing conditions.

The state of the stored ion ensemble is characterized by the plasma parameter $\Gamma_p = 1/(4\pi\epsilon_0) \times e^2/(a_{ws} kT)$ the

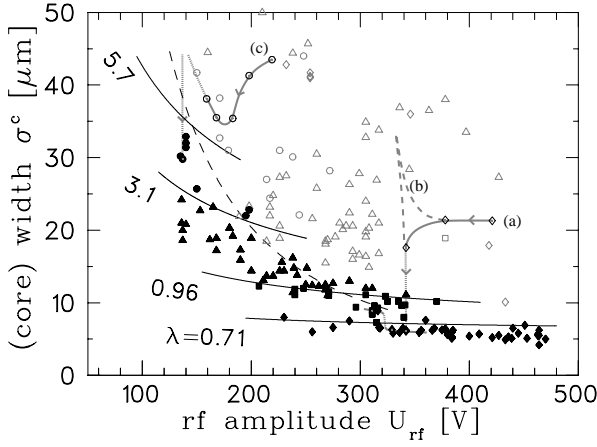


Figure 3: Correlation of the absolute width of stored ion beams (not corrected for the spatial resolution of the imaging system of about $5 \mu\text{m}$) and the applied rf voltage. Crystalline beams are depicted as filled (black), non-crystalline beams as open (grey) symbols. For crystalline beams, the solid contour lines of constant linear density λ separate regions of different crystal structure. At the dashed line, the energy contained in the driven transverse motion equalizes the melting temperature of crystalline beams. The grey lines illustrate transition paths (marked a,b,c) from the non-crystalline to the crystalline state (constant N).

ratio of the energy of the mutual Coulomb repulsion to the thermal energy. Large three-dimensional ensembles are expected to be in the crystalline state for $\Gamma_p > 178$ while surface dominated ensembles like ion beams may require higher values [26]. For the case of the sample crystalline beam presented above, the linear string ($\lambda \approx 0.4$), the velocity spread and thus the plasma parameter was measured [5] to $\Gamma_p > 500$, well within the crystalline regime.

SYSTEMATIC STUDIES

In Fig. 3, the transverse width σ^c of crystalline (filled symbols) and non-crystalline beams (open symbols) of different particle numbers N is plotted against the applied rf voltage U_{rf} . The phase transition from the non-crystalline to the crystalline state can be followed for two typical cases (grey lines). In (a), a reduction of the focusing strength, which was initially chosen rather high for the preparation of the beam, lead to a reduction of the rf heating of the gaseous beam and thus to a reduction of the transverse width down to the point where the crystallization occurred for a given cooling strength. Especially for beams of low linear density, the focusing strength had to be at first reduced to a point where the width of the beam expanded in order to reduce rf heating. A quick increase in the focusing strength, increasing the coupling between the longitudinal and the transverse motion, then lead to the crystallization of the beam (b), similar to the sample situation discussed above [5]. Both phases are possible for identical focusing conditions (hysteresis).

With the use of the relation $\sigma^c/a_{ws} \propto \sqrt{\lambda}$ (solid) contour lines are drawn for the threshold values of constant linear density [23]. In this way, the classification of the crystalline beams (filled symbols only) relies on the determination of the width of the beam σ^c and of the rf voltage U_{rf} [6], both of which are known to better than $\pm 5\%$. The alternative classification, based on the ion number N , is expressed by the different symbols.

Focusing requirements

Crystalline beams were observed to occur only in a curved band in the $(U_{rf} - \sigma^c)$ diagram (filled symbols in Fig. 3 [6]). Although the time-averaged focusing force is exactly canceled by the space charge force of a crystalline beam, the constituent ions are forced to oscillate in the transverse plane because of the discrete (or in this case time-dependent) periodic focusing [27]. Following Schiffer [17], an apparent temperature can be assigned to the spread of this transverse motion

$$\begin{aligned} 3kT_{app}^f &\approx \left(\frac{\Delta\sigma^c}{\sigma^c}\right)^2 \left(\frac{\sigma^c}{R}\right)^2 \frac{Q^4 m v^2}{2P^2} \\ &\approx \frac{e^2}{4\pi\epsilon_0 a_{ws}} \frac{\pi^2}{6} \frac{\lambda Q^2}{P^2}. \end{aligned} \quad (1)$$

This relation can be rewritten for an apparent plasma parameter $\Gamma_{app}^f \propto 1/(U_{rf}^{5/3} \sigma^c)^2 \propto (P/Q)^2/\lambda$.

The curvature of the band in Fig. 3 follows the dashed line, which is based on the argument that the apparent temperature equalizes the melting temperature, or that $\Gamma_{app}^f \approx 180$. Yet, it has to be emphasized that this driven periodic transverse motion in the quadrupole potential should not be automatically regarded as random or thermal motion. It was shown in simulations [19, 28] as well as in experiments [5, 18, 14] that the energy transfer from the periodic to the random motion is strongly suppressed compared to a non-crystalline ensemble. Thus, crossing this line does not immediately lead to the melting of a crystalline beam. On the other hand, for beams which are not sufficiently cold the coupling of collective motion into random motion is expected to increase and to hinder the crystallization.

The same curved bands of stability dominate the graphs in Fig. 4. In these $(\lambda - Q)$ diagrams, upper and lower limits of the focusing strength can be distinguished. The *lower* focusing limit appears to be rather constant for 3D beams but considerably raises for the lower dimensional crystalline beams. This effect is believed to be due to the specific cooling scheme, based on direct longitudinal laser cooling. Below the limiting focusing strength the ion density and thus the coupling between the transverse and the longitudinal degrees of freedom becomes too low to provide sufficient sympathetic transverse cooling. Thus, the tendency was to raise the focusing strength in order to increase the coupling up to the point where the depth of the transverse modulation of the crystalline beam sets the upper limit.

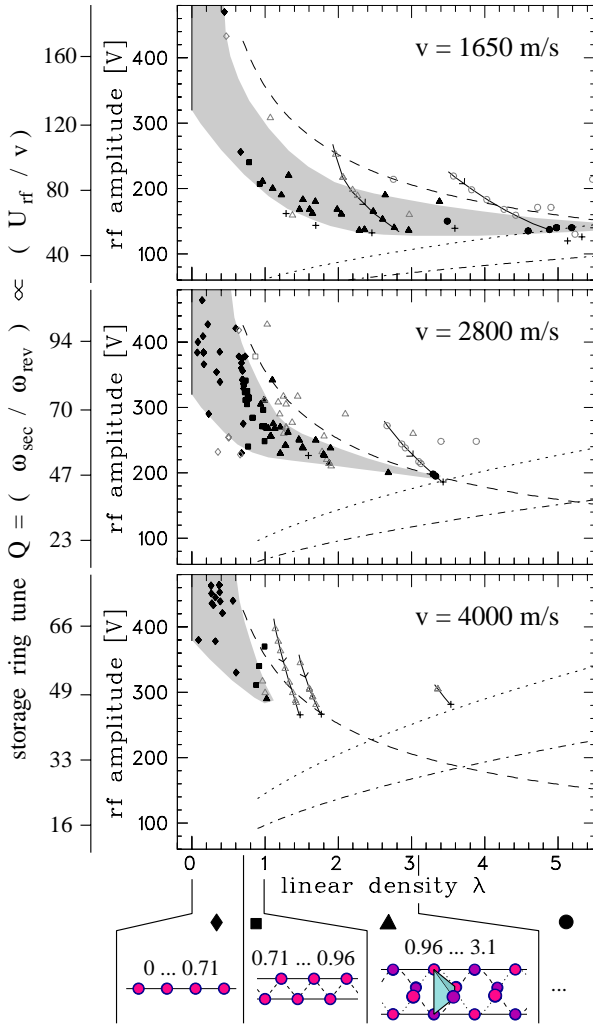


Figure 4: The focusing conditions for which crystalline ion beams of different linear density λ and thus of different structure (as illustrated below) were attainable in PALLAS are illustrated (grey shaded area) for three beam velocities. In each of the three graphs, the dashed line corresponds to the one in Fig. 3, the dotted and dash-dotted lines indicate the increasing influence of bending shear with rising velocity as explained in the text. Few solid lines indicate paths from the non-crystalline to the crystalline state or to beam losses (crosses), respectively.

This *upper* limiting focusing strength lies more than a factor of three below the value at which an excitation of bulk modes of the 3D crystalline beam is expected to occur. Their characteristic frequency is close to the plasma frequency $\omega_p = \sqrt{2} \omega_{sec}$ [25]. To avoid an excitation of such bulk modes in the oscillating fields of the storage ring, the lowest possible side-band of the driving frequency ($\Omega - \omega_p$) has to exceed twice the eigen-frequency ω_p or $\Omega > 2\omega_p$, which translates into the often discussed maintenance criterion $P > 2\sqrt{2} Q$ [17, 12]. This criterion is always fulfilled in PALLAS, where $P = \sqrt{8} Q/q$ and $q < 0.9$ for a sinusoidal rf driving voltage, but difficult to meet in the existing

heavy ion storage rings like TSR with ($Q = 2.8, P = 2$).

The above criterion is not restricted to crystalline beams but part of a more general approach to envelope instabilities of space-charge dominated beams. There, the latter condition corresponds to the first half-integer stop band (Mathieu instability) or, in other words, to the condition that the phase advance per lattice cell (or per rf period) must not exceed $2\pi/2\sqrt{2}$ [29, 30]. For emittance dominated (non-crystalline) beams, the phase advance per unit cell has to remain below $\pi/2$ [29, 30]. This criterion is important for the generation of crystalline beams starting from the gaseous phase and independent from the treatment of heating due to intra-beam scattering.

Bending shear

In addition to the previous presentation, the focusing conditions are now discussed for the three different beam velocities, depicted in the three separate graphs of Fig. 4. Obviously, crystalline beams of higher linear density could only be attained for the lowest beam velocity of $v = 1650 \text{ ms}^{-1}$. For higher beam velocities, and especially for $v = 4000 \text{ ms}^{-1}$, the beams were lost when the focusing strength was decreased into a region where crystalline beams had been attainable at lower velocities. Surprisingly, the lower focusing limit for the highest linear densities seems to appear at a tune of $Q \approx 45$ independent from the beam velocity.

Continuous bending of a crystalline beam extending into the horizontal plane ($\lambda > 1$) implies that the beam has to propagate with constant angular velocity to maintain its crystalline order [2, 17, 19]. The consequence of cooling the beam to constant linear velocity was illustrated by Schiffer [17] assigning an apparent temperature T_{app}^s to the mean centrifugal energy spread of the beam

$$3k_B T_{app}^s \approx \left(\frac{\sigma^c}{R} \right)^2 \frac{mv^2}{2} \approx \frac{e^2}{4\pi\epsilon_0 a_{ws}} \frac{4\pi^2}{9} \frac{\lambda}{Q^2}, \quad (2)$$

which can be related to an apparent plasma parameter as $\Gamma_{app}^s \approx 0.7 Q^2/\lambda$. When the beam is laser-cooled to constant linear velocity, this energy spread is fully transferred into random motion. This condition translates into the lower limit of the focusing strength as a function of the linear density, that is indicated by the dash-dotted lines in Fig. 4. It rises with increasing beam velocity in the same way as the experimental observations. This agreement is emphasized by the dotted lines which result from a multiplication of the latter limit by a factor of 1.5. The factor could be interpreted as taking into account only the transverse degrees of freedom in Eq. 2. It seems that, at present, bending shear prohibits the attainment of large crystalline structures already above velocities of around 2500 m/s in PALLAS.

However, to a certain degree, an already existing crystalline beam has been expected to withstand the bending due to its natural shear elasticity, characterized by the secular frequency ω_{sec} divided by λ [2, 17]. In this model,

the condition for a crystalline beam to resist bending shear becomes $Q > \lambda$, as the characteristic frequency (ω_{sec}/λ) has to remain higher than the driving revolution frequency ω_{rev} . Thus, no evidence for this ‘stiff beam limit’ has been found in the present experiments.

Cooling the ion beam to constant angular velocity could help to unambiguously decipher the role of bending shear in the observed velocity dependence of the lower focusing limit. Due to the comparatively low ion velocity in PAL-LAS, this cooling scheme could be accomplished by merging the ion and laser beams inside a segmented drift tube similar to the method, realized earlier for the measurement of the longitudinal velocity spread [5]. In the fringe field of a segmented drift tube, the change in ion energy slightly depends on the displacement from the ideal ion orbit so that constant angular velocity can be transformed into constant linear velocity and vice-versa. The ion beam can be cooled to constant linear velocity locally inside the drift tube and propagate at constant angular velocity outside.

CONCLUSIONS

Crystalline ion beams of different structure were attained starting from non-crystalline beams, which were subjected to longitudinal laser cooling. Integer-tune stop-bands had to be crossed when the secular motion was frozen out. Promisingly, no effect of this forbidden crossing of resonances was experienced. For the specific laser cooling scheme, the coupling between transverse and longitudinal motion came out to be crucial especially for the lower-dimensional beams and to require higher focusing strength. Direct transverse cooling - tough non-trivial to achieve [31] - should improve this situation [7].

The coupling of the driven transverse motion into thermal motion seems to set an upper limit ($Q \propto \sqrt{\lambda}$) to the applicable confinement strength. This limit was observed to be about a factor of three lower than the established maintenance criterion $P > 2\sqrt{2} Q$, a fact that further raises the demands on the ‘smoothness’ of the lattice of a high-energy storage ring.

With cooling to linear velocity, bending shear gains importance with increasing beam radius. The first experimental findings, that the attainment of large crystalline beams becomes more difficult (or even impossible) with rising ion beam velocity agrees with simple models ($Q \propto 1/\sqrt{\lambda}$). Scaling the present result according to Eq. 2, storage rings of several 100m radius (and considerably high tune) are required to maintain helical structures at about $v/c \approx 0.1$ unless a method for cooling to constant angular velocity can be found.

More generally, bunched beam laser cooling will be the method of choice for the anticipated attainment of dense crystalline ion strings at relativistic energies, as the huge Doppler-shift only allows for counter-propagating laser and ion beams. A test experiment is currently prepared for the ESR of GSI, where a beam of Li-like C^{3+} ions at a velocity of $v/c = 0.47$ will be subjected to a combination

of transverse electron and longitudinal laser cooling. With the operation of larger heavy ion synchrotrons (SIS 300 at GSI), laser cooling of Li-like ions of the order of uranium becomes possible with fascinating possibilities for the forward scattering of laser light into the keV range. On the other hand, the application of refined cooling techniques could strongly enhance the luminosity of radioactive beam colliders, presently under discussion.

REFERENCES

- [1] J.P. Schiffer and P. Kienle, Z. Phys. A **321**, 181 (1985).
- [2] J.P. Schiffer and A. Rahman, Z. Phys. A **331** 71 (1988).
- [3] For an overview, see D. Habs and R. Grimm, Ann. Rev. Nucl. Part. Sci. **45**, 391 (1995) and refs. in [5, 7].
- [4] *Crystalline Beams and Related Issues*, D.M. Maletic and A.G. Ruggiero (eds.), World Scientific, Singapore, (1996).
- [5] T. Schätz, et al., Nature **412**, 717 (2001).
- [6] U. Schramm, et al., Phys. Rev. E **66** 036501 (2002).
- [7] U. Schramm, et al., Plasma Phys. Control. Fusion **44**, B375 (2002).
- [8] U. Schramm, et al., Phys. Rev. Lett. **87**, 184801 (2001).
- [9] U. Schramm, et al., Physics Scripta (at press 2003) and M. Bussmann, et al., J. Phys. A, (at press 5/2003).
- [10] S. Schröder et al., Phys. Rev. Lett. **64**, 2901 (1990) and J.S. Hangst, et al., Phys. Rev. Lett. **67**, 1238 (1991).
- [11] Q. Spreiter, et al., Nucl. Instr. Meth. A **364**, 239 (1995) and M. Seurer, et al., Hyp. Int. **99**, 253 (1996).
- [12] J. Wei, et al., in [4], p 229 (1996).
- [13] M. Steck, et al., Phys. Rev. Lett. **77**, 3803 (1996).
- [14] M. Steck, Proc. PAC 2001 (Chicago, USA) TOAA002 (2001) and M. Steck, et al., J. Phys. B **36**, 991 (2003).
- [15] H. Danared, et al., Phys. Rev. Lett. **88**, 174801 (2002).
- [16] U. Eisenbarth, et al., Hyp. Int. **127**, 223 (2000).
- [17] J.P. Schiffer, in [4], p 217 (1996).
- [18] U. Schramm, et al., J. Phys. B **36**, 561 (2003).
- [19] J. Wei, et al., Phys. Rev. Lett. **80**, 2606 (1998).
- [20] N. Madsen, et al., Phys. Rev. Lett. **87**, 274801 (2001).
- [21] T. Schätz, et al., Applied Physics B **76**, 183 (2003).
- [22] R.W. Hasse et al., , Annals of Phys. **203**, 419 (1990).
- [23] G. Birkel, et al., Nature **357**, 310 (1992).
- [24] M. Drewsen, et al., Phys. Rev. Lett. **81**, 2878 (1998).
- [25] D.H.E. Dubin, T.M. O’Neil, Rev. Mod. Phys. **71**, 87 (1999).
- [26] J.P. Schiffer, Phys. Rev. Lett. **88**, 205003 (2002).
- [27] The amplitude of the rf driven micro-motion amounts to $\Delta r \approx \sqrt{2}\omega_{sec}r/\Omega \propto 1/\Omega^2$.
- [28] J.P. Schiffer, et al., Proc. Natl. Acad. Sci. USA **97**, 10697 (2000).
- [29] I. Hofmann, in [4], p. 3 (1996).
- [30] S.Y. Lee and H. Okamoto, Phys. Rev. Lett. **80**, 5133 (1998).
- [31] I. Lauer, et al., Phys. Rev. Lett. **81**, 2052 (1998).